Profiling target engagement and cellular uptake of cRGD-decorated clinical-stage core-crosslinked polymeric micelles

Federica De Lorenzi (fdelorenzi@ukaachen.de)
RWTH ExMI: Rheinisch-Westfalische Technische Hochschule Aachen Institute for Experimental Molecular Imaging

Larissa Yokota Rizzo
RWTH ExMI: Rheinisch-Westfalische Technische Hochschule Aachen Institute for Experimental Molecular Imaging

Rasika Daware
RWTH ExMI: Rheinisch-Westfalische Technische Hochschule Aachen Institute for Experimental Molecular Imaging

Alessandro Motta
RWTH ExMI: Rheinisch-Westfalische Technische Hochschule Aachen Institute for Experimental Molecular Imaging

Maike Baues
RWTH ExMI: Rheinisch-Westfalische Technische Hochschule Aachen Institute for Experimental Molecular Imaging

Matthias Bartneck
Uniklinik RWTH Aachen: Universitatsklinikum Aachen

Michael Vogt
Uniklinik RWTH Aachen: Universitatsklinikum Aachen

Marc van Zandvoort
Maastricht University Hospital: Maastricht Universitair Medisch Centrum+

Leonard Kaps
Universitat Mainz: Johannes Gutenberg Universitat Mainz

Qizhi Hu
Cristal Therapeutics

Marielle Thewissen
Cristal Therapeutics

Luca Casettari
University of Urbino: Universita degli Studi di Urbino Carlo Bo

Cristianne J.F. Rijcken
Cristal Therapeutics

Fabian Kiessling
RWTH ExMI: Rheinisch-Westfalische Technische Hochschule Aachen Institute for Experimental Molecular Imaging
Alexandros Marios Sofias
RWTH ExMI: Rheinisch-Westfalische Technische Hochschule Aachen Institute for Experimental Molecular Imaging
Twan Lammers
RWTH ExMI: Rheinisch-Westfalische Technische Hochschule Aachen Institute for Experimental Molecular Imaging

---

Research Article

Keywords: Nanomedicine, tumor targeting, nanoparticles, core-crosslinked polymeric micelles, cyclic arginine-glycine-aspartic acid (cRGD), CriPec®

Posted Date: March 30th, 2022

DOI: https://doi.org/10.21203/rs.3.rs-1372856/v1

Version of Record: A version of this preprint was published at Drug Delivery and Translational Research on July 11th, 2022. See the published version at https://doi.org/10.1007/s13346-022-01204-8.

Abstract

Polymeric micelles are increasingly explored for tumor-targeted drug delivery. CriPec® technology enables the generation of core-crosslinked polymeric micelles (CCPM) based on thermosensitive (mPEG-b-pHPMAmLac$_n$) block copolymers, with high drug loading capacity, tailorable size, and controlled drug release kinetics. In this study, we decorated clinical-stage CCPM with the $\alpha_v\beta_3$ integrin-targeted cyclic arginine-glycine-aspartic acid (cRGD) peptide, which is one of the most well-known active targeting ligands evaluated preclinically and clinically. Using a panel of cell lines with different expression levels of the $\alpha_v\beta_3$ integrin receptor and exploring both static and dynamic incubation conditions, we studied the benefit of decorating CCPM with different densities of cRGD. We show that incubation time and temperature, as well as the expression levels of $\alpha_v\beta_3$ integrin by target cells, positively influence cRGD-CCPM uptake, as demonstated by immunofluorescence staining and fluorescence microscopy. We demonstrate that even very low decoration densities (i.e., 1 mol % cRGD) result in higher engagement and uptake by target cells as compared to peptide-free control CCPM, and that high cRGD decoration densities do not result in a proportional increase in internalization. In this context, it should be kept in mind that a more extensive presence of targeting ligands on the surface of nanomedicines may affect their pharmacokinetic and biodistribution profile. Thus, we suggest a relatively low cRGD decoration density as most suitable for in vivo application.

Introduction

Polymeric micelles are versatile nanocarriers, extensively used for the encapsulation and delivery of hydrophobic drugs. Such drugs can be entrapped and stabilized either via physical (e.g., hydrophobic interactions and π-π stacking) or chemical interactions (e.g., covalent core-crosslinking) [1, 2]. Formulations based on CriPec® technology are core-crosslinked polymeric micelles (CCPM) based on thermosensitive methoxy poly(ethylene glycol)-*b*-poly[N-(2-hydroxypropyl) methacrylamide lactate] (mPEG-b-pHPMAmLac$_n$) block copolymers. During the manufacturing of CriPec® CCPM, the block copolymers self-assemble into core-shell structures in aqueous solutions and are then crosslinked in the micellar core by means of free radical polymerization. During this process, hydrophobic drug molecules are co-crosslinked, resulting in covalent attached in cthe stabilised micellar core via hydrolysable linkages that enable release of native drug molecules at the target site with predetermined kinetics [3].

Covalent core-crosslinking results in enhanced in vivo stability and prolonged circulation half-life times, allowing for an efficient accumulation at the target site [1, 4, 5], in contrast to conventional polymeric micelles that typically disintegrate faster in systemic circulation upon intravenous (i.v.) administration. These benefits have been apparent in preclinical image-guided drug delivery set-ups where fluorescence-labeled CCPM were tracked in vivo via hybrid fluorescence tomography - computed tomography. In this set-up, CCPM achieved a tumor accumulation of 18.6%ID/g at 48 h post i.v. injection in a triple-negative breast cancer model in mice [6]. Extending preclinical evaluation, CriPec®-based CCPM technology has been clinically trialed. Docetaxel-entrapped CCPM, also known as CPC634, is the clinically most

advanced nanomedicine manufactured by Cristal Therapeutics. CPC634 has undergone Phase I and II clinical trials in the Netherlands, Belgium and UK, for assessing the micelles' pharmacokinetic (PK), biodistribution (BD), and accumulation in solid tumors and metastases (NCT03712423, NCT02442531), as well as to evaluate its safety and efficacy in platinum-resistant ovarian cancer (NCT03742713) [7–9]. Of note, the administration of CPC634 resulted in a four-fold higher tumor accumulation of docetaxel in advanced solid tumors in patients, as compared to the administration of free docetaxel [7].

All above-mentioned preclinical and clinical studies have been executed employing passively targeted CCPM. Passive targeting to malignant lesions has been described to occur due to disease-specific hyperpermeable blood vessels and defective lymphatic drainage. The combination of passive barrier-crossing and retention has been described by Matsumura and Maeda in 1986 as the Enhanced Permeability and Retention (EPR) effect [10]. While in the last couple of decades passive targeting has been mostly attributed to vascular leakiness, novel image-guided research has discovered the extravasation of passive targeting nanomedicines to be a cumulative effect of vascular bursts, myeloid cell-dependent vascular ruptures, as well as endothelial transcytosis [11–14]. Furthermore, the retention of nanomedicines at malignant sites have been described to be secondary to phagocytic uptake by tumor-associated macrophages (TAM) as a mechanism of nanoparticle retention [15].

In addition to EPR and other passive targeting mechanisms, decoration of nanomedicines with targeting ligands offers the possibility for active targeting by capitalizing on the molecular specificity of a ligand or an antibody / antibody fragment for a receptor upregulated by the cell population target. Such nanoparticle surface decorations can potentiate targeting of a drug to a specific tissue, cell type or subcellular compartment [16]. Even though this concept appears straightforwardly beneficial, actively targeted nanomedicines have not yet been approved for use in the clinic, due to overall suboptimal in vivo performance and unfavorable PK profiles, due to poor biological barriers penetration, protein corona formation, and recognition by the mononuclear phagocyte system (MPS) [16, 17]. In this regard, various parameters during the preparation procedure may crucially affect the in vivo performance of active targeting nanomedicine, e.g., ligand decoration procedures, surface decoration density, ligand decoration density, and exposure of the ligand at the outer shell of the nanoparticle [18–21].

In this study, we decorated CCPM with an arginine-glycine-aspartic acid peptide (i.e., RGD; note that the cyclic RGDfK pentapeptide was used), as it is one of the most well-known active targeting ligands tested both preclinically and clinically [22–28], and holds promise for targeting not only cancer cells, but also activated endothelial cells [29], stromal cells [30] and immune cells [31]. By producing CCPM with three different decoration densities of cRGD (0, 1, 3.6 and 5 mol%) and a control composition without cRGD decoration, we aimed at assessing the biological activity of the ligand when anchored on the nanoformulation, as well as at examining whether higher decoration densities are meaningful for improving target binding and internalization. Of note, too high levels of ligand decoration density are known to deteriorate in vivo performance due to high recognition by phagocytes and off-target deposition in clearance organs [32, 33].

Our experimental set-up included the incubation of four cell lines / primary cells (A431, HUVEC, activated HUVEC, 4T1) that are well-known to display different $\alpha_v\beta_3$ integrin expression levels (**Fig. S1** – $\alpha_v\beta_3$ integrin is the receptor-target of cRGD ligand) with all four CCPM variations (0, 1, 3.6 and 5 mol% cRGD), at various temperatures (4 and 37^{o}C), time points (4, 24 and 72 h), and incubation conditions (static and under flow). The assessment of CCPM engagement, target binding, and uptake by cells was validated via histology, fluorescence microscopy, multiphoton microscopy, and flow cytometry.

The outcomes of this study improve our understanding on the effect of ligand decoration densities in targeting a given biological system, and they promote progress and improvements in developing actively targeted cancer nanomedicines.

Materials And Methods

Rhodamine-labeled core-crosslinked polymeric micelles

Rhodamine-labeled block copolymer was synthesized by conjugating rhodamine B (excitation = 550 nm) to the terminal hydroxyl groups of polymer lactate side chains, via formation of an ester bond. Partially methacrylated $mPEG_{5000}$-b-$pHPMAmDP_1DP_2$ block copolymer (21.5 kDa, 10 mol% methacrylated, 0.140 mmol) was reacted with rhodamine B (0.698 mmol) using N,N'-Dicyclohexylcarbodiimide (DCC) (0.698 mmol) and 4-(dimethylamino)pyridine (DMAP) (0.698 mmol) in Dichloromethane (DCM) (30 mL) at room temperature. After 24 hours, DCM was evaporated and the remaining reaction mixture was dissolved in milliQ water (150 mL), followed by dialysis (MWCO 12-14 kDa) against acetonitrile (ACN)/milliQ water (50v/50v) at 4^{o}C to remove unreacted rhodamine molecules, and subsequently freeze-dried to obtain rhodamine-labelled block copolymer as a pink powder. Consequently, a mixture of synthesized rhodamine-labelled block copolymer (23 w%) and methacrylated $mPEG_{5000}$-b-$pHPMAmDP_1DP_2$ block copolymer (77 w%) were used to synthesize rhodamine-labelled core-crosslinked polymeric micelles, following a previously reported protocol [1] DCC and DMAP were purchased from Sigma-Aldrich. Dichloromethane DCM and ACN were obtained from Actuall Chemicals. Azide-PEG_{5000}-OH was purchased from Rapp Polymere GmbH. Rhodamine B was purchased from Acros Organics. To functionalize CPPM with cRGD, the cRGDfk-targeting ligand was conjugated to the azide moiety of the nanoparticles via BCN conjugation [1,4,34]. Four batches of cRGD-conjugated rhodamine-labelled CriPec® (empty) core-crosslinked polymeric micelles (CCPM) were provided by Cristal Therapeutics (Maastricht, The Netherlands), containing 0, 1, 3.6, and 5 mol% cRGD. All micelles were characterized via DLS by the manufacturer displaying a narrow size distribution of 35 nm in diameter. CCPM were dispersed in 180mM HEPES buffer pH 7.0, hence, batches were stored at 4°C.

In vitro cell culture

A431 epidermoid squamous cancer cells were purchased from ATTC® (Manassas, VA) and cultured in RPMI medium (Invitrogen; Darmstadt, Germany) supplemented with 10% FCS (Fetal Calf Serum;

Invitrogen, Darmstadt, Germany) and 1% Penicilinin/Streptavidin (Pen/Strept; Invitrogen, Darmstadt, Germany). HUVEC (Human umbilical vein endothelial cells) were purchased from Promocell® (Heidelberg, Germany) and cultured with endothelial cell growth medium (Endopan 3 Pan-Biotech® 500ml) supplemented with 15 ml FCS, 0.1 ml Hydrocortison, 0.5 ml EGF, 0.5 ml Ascorbic acid, 0.5 ml VEGF, 0.5 ml FGF2, 0.5 ml Heparin, and 5 ml P/S, 5ml Gentamicin sulfate). As primary cells, HUVEC were only used up to passage number 8. 4T1 murine triple-negative breast cancer cells were purchased from ATTC® (Manassas, VA) and cultured in RPMI medium (Invitrogen; Darmstadt, Germany) supplemented with 10% FCS (Fetal Calf Serum; Invitrogen, Darmstadt, Germany) and 1% Penicillin/Streptavidin (Pen/Strept; Invitrogen, Darmstadt, Germany). Cell passaging was performed following standard cell culture protocols in T75 cell culture flasks (Cell Star, Greiner, Germany) upon 70-80% confluency. Cultures were maintained in a 37^{o}C incubator with 5% CO_2 and 95% relative humidity.

Nanoparticle uptake assay under static cultivation conditions

The cell uptake of CCPM was tested at different incubation times (4, 24 and 72 h) and at different incubation temperature (4°C, 37°C). Cells were seeded in 24-well tissues culture plates (Falcon®) pre-filled with glass coverslips (Thermoscientific®) with a cell seeding concentration of 10000 cells per well for the 24 h incubation time point and 1000 cells per well for the 72 h incubation time point. The 4 CCPM batches were diluted in PBS and used at a concentration of 0.1 mg/ml in culture medium. HUVEC were activated by TNFα (PromoKine® Recombinant Human Tumor Necrosis Factor alpha, E.Coli derived 10µl) at a concentration of 4 ng/mL for 4 hours following a previously published protocol in [35]; before incubation with CCPM, TNFα enriched medium was removed and fresh medium with CCPM was added. For the 72 h incubation time point at 37°C, in addition to activated HUVEC (HUVEC^{+}), quiescent HUVEC (HUVEC^{-}) were also used. At the end of the experiment, coverslips were rinsed with PBS, cells werefixed with 4% paraformaldehyde (PFA) for 20 minutes at room temperature (RT) and subjected to histology.

Nanoparticles uptake assay under dynamic flow conditions

To validate the binding and uptake of control and cRGD-decorated CCPM under fluidic shear stress in vitro, only control and 5 mol% cRGD CCPM were used at a concentration of 0.1 mg/mL in medium. 200 000 cells were seeded on 35-mm Petri dishes. Quiescent HUVEC were tested as additional negative control for the expression of integrin receptors. Petri dishes were placed into a customized parallel-wall flow chamber in a custom silicon tube perfusion system (standard silicon tubing, 0.76 mm inner diameter; Helixmark) [36]. Using a peristaltic pump (Gilson®), the flow rate was set with a speed of 0.20-0.25 ml/min for 10 minutes, followed by 5 minutes washing with PBS. Cells were then fixed with PFA and further processed for histology.

Internalization studies with LysoTracker and flow cytometry

4T1 cells were cultured and incubated with non-targeted and cRGD-decorated CCPM for 24 h at 37°C. Cells were then stained for 30 min (37°C) for the lysosomial compartment with Lysotracker Green diluted in PBS, according to supplier´s protocol. For Flow Cytometry, 4T1 cells were seeded into 24-well plates (100000 cells/ml per well) and incubated at 37°C overnight. Cells were subsequentially incubated with CCPM for 24 h at 37°C, washed, trypsinized, and cell suspension centrifuged at 1200 rpm for 5 min. After supernatant removal, the cell pellet was resuspended in ice-cold PBS and analyzed with the BD FACSCanto II Flow cytometry system (Becton, Dickinson and Company, US).

Histological analysis

Cells exposed to control and cRGD-CCPM were washed with PBS, fixed with 4% PFA for 20 min at RT, and washed again thrice with PBS. Primary antibodies (abcam® ab7166) were diluted in 12% bovine serum albumin (BSA) (PAN Biontech, Germany) and applied for 1 h at RT. Excess antibody was removed via three consecutive PBS washes, and coverslips were subsequetly incubated with the respective secondary antibodies, also diluted in 12% BSA (Cy3-anti-rat (Dianova# 115-165-166). Unbound antibodies were removed via PBS washes, coverslips were mounted with Mowiol 4-88 (Carl-Roth, Germany) into glass slides, and the glass-covered to be stored at 4°C. For staining of the cytoskeleton and of nuclei, phalloidin (Promofluor® 488 Phalloidin, Promokine) and DAPI (1:500; Merck, Germany) were diluted in 12% bovine serum albumin (BSA) (PAN Biontech, Germany) and applied for 1 h at RT. Coverslips were washed with PBS and mounted on object slides with Mowiol and stored at 4°C.

Fluorescent microscopy image anaylsis

For imaging cells incubated with CCPM and lysotracker®, all images were acquired with a fixed exposure times using a Zeiss® AxioImager M2 microscope (20x objective, with a numerical aperture of 0.8) or an inverted Leica DMI6000 B (Leica microsystems, Germany, 40x objective with a numerical aperture of 0.95). For rhodamine and lysotracker detection fixed exposure times of 1500 ms and 1200 ms respectively, were used; for DAPI/Hoechst and Phalloidin exposure times were comprised in a range between 19 and 25 ms for the firsts, and between 50 and 100 msfor the latter. The image processing and quantification of area fraction percentage (AF %) for the fluorescence signals associated with rhodamine and and lysotracker® were performed using Axiovision LE and Leica Las AF software, respectively.

Two-photon laser scanning microscopy

To detect the 3D binding and uptake of targeted and non-targeted nanoparticles by 4T1 cells and assess their internalization process, two-photon laser scanning microscopy (TPLSM) was used.The FV1000MPE Multiphoton Microscopy System (Olympus, Hamburg), was equipped with a Mai TaiDeepSee pulsed

Ti:Sapphire laser, and a 25× water dipping objective with a Numerical Aperture of 0.95. The excitation wavelength was set to 800 nm with 15% power for the image acquisition. This wavelength allowed excitation of all probes. For the detection of fluorescence signal one photo multipliertube per dye was used and the filters adjusted correspondingly to emission spectra. Image acquistion was executed with Kalman filtering, the following processing and 3D analysis were performed with the Imaris 7.4 software (Bitplane, Zurich).

Statistical analysis

All data are presented as mean ± standard error (SD). The number of experimental replicates is indicated in figure legends. Data were tested for levels of significance using a Kruskal-Wallis one-way ANOVA followed by Dunn´s multiple comparison correction test or by a two-tailed non-parametric Mann-Whitney ´s test when only two groups were compared. Statistical analyses and data plotting were performed with GraphPad Prism 9.0 (San Diego, CA, USA). Levels of significance are indicated as follows: * $p < 0.05$; ** $p < 0.01$; *** $p < 0.001$.

Results And Discussion

cRGD-decorated CCPM display time-, temperature- and ligand density-dependent uptake in $\alpha_v\beta_3$ integrin-expressing cell lines

A panel of four cell lines characterized by increasing expression levels of $\alpha_v\beta_3$ integrins (**Fig. S1**) was compiled: A431 (human epidermoid carcinoma cell line, $\alpha_v\beta_3$-integrin^{low} [37]), HUVEC (model of quiescent endothelial cells in blood vessels of healthy tissues, $\alpha_v\beta_3$-integrin^{mid}; HUVEC$^-$); TNFα–activated HUVEC (model of active and proliferative endothelial cells in angiogenic tumor blood vessels, $\alpha_v\beta_3$-integrin^{high}; HUVEC$^+$ [38]), and 4T1 (murine triple-negative breast cancer cells, $\alpha_v\beta_3$-integrin^{high}). Our first experiment involved the incubation of A431, HUVEC$^+$, and 4T1 cell lines with all four cRGD-conjugated rhodamine-labelled CCPM formulations (0, 1, 3.6, and 5 mol% cRGD) for short periods of time, i.e. 4 and 24 h, at both 4^{o}C and 37^{o}C. In this case, 4 ^{o}C were selected to quantify the level of energy independent binding [39]. The degree of uptake was quantified as rhodamine area fraction % (AF%) in fluorescence microscopy images (**Fig. 1, 2, S2, S3, S4**).

A431 cells displayed a low uptake of all four CCPM formulations at both temperatures of incubation, with only minor uptake deviations among the different groups. The uptake ranged between 6.9-7.9 AF% (4 h – 4^{o}C), 7.5-9.8 AF% (24 h – 4^{o}C), 8.5-10.8 AF% (4 h – 37^{o}C), and 8.9-11.7 AF% (24 h – 37^{o}C), exemplifying that in integrin-negative cells, longer incubation time and higher temperature contributed only very marginally to uptake enhancement. When comparing the different CCPM formulations within the same incubation time and temperature group, all 3 cRGD-decorated formulations displayed a similar uptake, with only a small and not statistically significant increase in uptake in comparison to the cRGD-free

control formulation. Exemplarily, 5% cRGD decoration contributed to an additional 1.0, 1.8, 2.3, and 2.8 AF% for the 4 h – 4^{o}C, 24 h – 4^{o}C, 4 h – 37^{o}C, and 24 h – 37^{o}C group, respectively, in comparison to 0% decoration (**Fig. 1, 2, S2**).

HUVEC^{+} cells, unlike A431 cells, displayed larger CCPM uptake deviations among the different incubation groups; a pattern that was expected considering the high $\alpha_v\beta_3$ integrin expression by this cell line upon TNFα activation. The uptake spanned between 2.8-7.6 AF% (4 h – 4^{o}C), 3.2-6.9 AF% (24 h – 4^{o}C), 4.1-10.6 AF% (4 h – 37^{o}C), and 3.2-13.0 AF% (24 h – 37^{o}C), showing that higher temperature contributed to more efficient uptake. Comparing the uptake of the different CCPM formulations uptake within the same incubation time – temperature group, cellular internalization was consistently elevated in a step-wise manner, in line with cRGD density. For example, after 24 h of incubation at 37^{o}C, the CCPM uptake was 3.2, 7.1, 10.4, and 13.0 AF% for 0, 1, 3.6, and 5% cRGD, respectively. Overall, CCPM uptake was found to be significantly higher for 3.6 and 5% cRGD versus 0% cRGD at various incubation conditions (**Fig. 1, 2, S3**), thus proving active uptake mediated by the integrin receptor and the additional uptake upon increasing cRGD on CCPM surface.

4T1 cells displayed the highest levels of internalization of CCPM in comparison to the other cell lines. Specifically, unlike the 6.9-11.7 and 2.8-13.0 AF% uptake-ranges observed by A431 and HUVEC^{+}, 4T1 cells presented with values as high as 9.3-16.0 AF% (4 h – 4^{o}C), 12.6-25.5 AF% (24 h – 4^{o}C), 10.3-18.4 AF% (4 h – 37^{o}C), and 13.5-28.3 AF% (24 h – 37^{o}C). Incubation time was found to be essential for promoting CCPM internalization, while temperature increase less prominently contributed to uptake enhancement. As expected, and in line with the observations for HUVEC^{+}, increasing the density of cRGD decoration corresponded with an increase in cellular uptake, with 5% cRGD conjugation resulting in significant uptake enhancement in comparison to control micelles for three out of four test condition (i.e, 24 h – 4^{o}C, 4 h – 37^{o}C, and 24 h – 37^{o}C). The group with the largest uptake differences was the 24 h – 37^{o}C group, where the CCPM uptake was 13.5, 17.9, 23.1, and 28.3 AF% for the 0, 1, 3.6, and 5% cRGD, respectively (**Fig. 1, 2, S4**).

Together, these findings demonstrate that cRGD-decoration does not improve the uptake of CCPM by $\alpha_v\beta_3$-integrin^{low} cells. As compared to non-decorated CCPM, cRGD-decorated CCPM are taken up to a greater extent by $\alpha_v\beta_3$-integrin^{high} cells (4T1 and HUVEC^{+}), in a time-, temperature- and ligand density-dependent manner.

Long incubation time points do not result in additional cRGD-CCPM uptake, while TNFα- activation enhances nanoparticle uptake by endothelial cells.

The second experimental setup examined the uptake of the four CCPM formulations after a longer incubation time of 72 h. In this experiment, in addition to A431, HUVEC^{+}, and 4T1 cells, also non-activated HUVEC (HUVEC^{-}) were included. This addition allowed for investigating the effect of TNFα-mediated activation in CCPM uptake, because TNFα-based activation cause, among other effects, an increase in

integrin expression by endothelial cells [40]. By comparing the uptake patterns between incubation for 24 h at 37^{o}C (**Fig. 1, 2**) and incubation for 72 h at 37^{o}C (**Fig. 3, S5**), it became evident that similar trends are observed with respect to the uptake of the four CCPM. Specifically, the uptake of all CCPM formulations by A431 cells was spanning within a short range, i.e., 6.6-7.6 AF%, with minor differences among the control and the cRGD-decorated formulations (**Fig 3**). Conversely, after 72 h of incubation at 37^{o}C, HUVEC^{+} and 4T1 cells had efficiently internalized the CCPM that displayed the highest density of cRGD-decoration; a pattern also observable at shorter incubation times. In case of HUVEC^{+}, the uptake was found to be 5.4, 9.3, 11.1, and 13.9 AF%, for 0, 1, 3.6, and 5% cRGD, respectively, with the values for 3.6 and 5% cRGD being significantly higher than for the cRGD-free control CCPM. Analogously, for 4T1 cells, the uptake was quantified at 13.2, 19.2, 21.3, and 26.0 AF% for the 0, 1, 3.6, and 5% cRGD, respectively, with the 5% cRGD CCPM displaying significantly higher uptake than control (**Fig. 3**).

In this experiment, a key point was to compare cRGD-targeted CCPM uptake between activated and non-activated HUVEC. For all four formulations, activated HUVEC displayed a higher degree of CCPM internalization in comparison to non-activated cells. The values of higher uptake of CCPM by HUVEC^{+} were quantified to range between 0.8 to 3.1 AF% as compared to the uptake by quiescent HUVEC. Specifically the values of uptake of cRGD CCPM were of 5.4, 9.3. 11, and 14 for HUVEC^{+} for the 0, 1, 3.6, and 5% cRGD formulations respectively and of 4.6, 7.1, 9.6, and 10.8 AF% for the 0, 1, 3.6, and 5% cRGD for quiescent HUVEC (**Fig. 3**). Although these differences are not statistically significant when the values of AF% are compared head-to-head by cRGD decoration density for quiescent and activated, they are also not trivial, highlighting that TNFα-activated HUVEC have a propensity to internalize nanomaterial at higher extent. Such observation alludes to the more phagocytotic behavior of angiogenic / inflammatory endothelium versus the quiescent nature of mature non-inflammatory endothelium. This preferential uptake of nanomaterial by angiogenic / inflammatory endothelium versus quiescent endothelium has been already observed in vivo by us [13], where the angiogenic endothelium in 4T1-bearing animals, displayed a 1.7 fold increase of cRGD nanoparticles uptake as compared to non-angiogenic endothelium.

Dynamic cultivation conditions benefit cRGD-CCPM uptake by target cells

Our next experiment aimed at exploring how the parameter shear stress influences the recognition of the $\alpha_v\beta_3$ integrin by the various cRGD nanoformulations. To this end, we compared the internalization of 0 and 5% cRGD CCPM in A431, HUVEC^{-}, HUVEC^{+}, and 4T1 cells after a very short incubation time of 10 min at 37^{o}C under dynamic flow conditions, using a microfluidic chamber assay established previously [36]. This assay was used to study cRGD-CCPM internalization efficiency in a more realistic scenario as compared to the static set-up described above.

Dynamic incubation of all four cell types with control and 5% cRGD-decorated formulations showed similar uptake of the two formulations in A431 cells, but clearly higher uptake of the 5% cRGD formulation by HUVEC^{-}, HUVEC^{+}, and 4T1 cells (**Fig. 4A, S6**). Quantification of the images corroborated the qualitative observations, with for 0 and 5% cRGD CCPM uptake values of 6.6 and 7.9 AF% in A431

cells, 4.2 and 7.9 AF% in HUVEC$^-$, 5.0 and 13.2 AF% in HUVEC$^+$, and 7.8 and 15.7 AF% in 4T1 cells; all differences were found to be statistically significant (**Fig. 4B**). As for previous experiments conducted under static cultivation condition for 72 h at 37 ^oC, a key comparison was the one between quiescent HUVEC and HUVEC$^+$ concerning the cRGD-CCPM uptake efficiency. The values of cRGD-CCPM uptake was of 7.9% for HUVEC$^-$ and 13% for HUVEC$^+$ respectively, with a P value of 0.0242 following a Mann-Whitney´s non-parametric, two-tailed t-test, thus confirming a statistically significant higher uptake of cRGD-CCPM by angiogenic / inflammatory endothelium as compared to quiescent endothelium.

This experiment under flow conditions clearly showed superior targeting ability of 5% cRGD CCPM in case of $\alpha_v\beta_3$ integrin expressing cells. Also, the rhodamine AF% quantified for HUVEC$^+$ is slightly lower compared to the same recorded for 4T1, so the latter appears to be more keen to bind and internalize cRGD-CCPM. These results may likely be consequent to a combination of factors. First, a higher level of $\alpha_v\beta_3$ integrin expression by 4T1 cells compared to HUVEC$^+$ cells and second, the higher metabolic rate of tumor cells that is associated to faster integrin internalization and recycling. Considering an eventual in vivo translation of the current study and taking the above results under flow conditions into account, it is reasonable to assume that cRGD-CCPM would bind more efficiently to angiogenic endothelial cells in tumor vasculature than to quiescent endothelial cells in healthy tissues. This is in line with various reports in the literature [37,41–43].

Overall, the here presented experiments highlight efficient and rapid recognition of the $\alpha_v\beta_3$ integrin receptor by cRGD-decorated CCPM. This notion is in line with several in vitro observations, showing rapid and efficient integrin-mediated internalization already at 180 min post incubation with integrin positive cells [44]. In vivo observations obtained via e.g., intravital microscopy showed significant uptake of cRGD-decorated lipid nanoparticles by α_v and β_3 integrin subunit expressing immune cells already at very early time points post i.v. injection (i.e. 5, 10, 20 min) [13,18].

Analyzing CCPM nanoformulation internalization

Our next experiments aimed at unraveling the contribution of integrin-receptor targeting to the internalization of cRGD-conjugated CCPM by $\alpha_v\beta_3$-integrin^{high} 4T1 cancer cells. This was done because integrins - in addition to being popular membrane targets on several different cell types - are known to be efficient internalizers, to engage in endo/phagocytosis pathways, and to be rapidly recycled [45,46]. For this purpose, upon incubation with control and cRGD-decorated CCPM for 24 h at 37^oC, 4T1 cells were stained with lysotracker® to visualize endosomal-lysosomal trafficking. On live-cell imaging, the co-localization of CCPM (red) with endosomes/lysosomes (green) produced a yellow/orange fluorescent signal in merged images, suggestive for CCPM cellular internalization (**Fig. 5A, S7**). In addition to this, the acquisition of 3D multiphoton microscopy images revealed the rhodamine-labelled nanoformulations, particularly the 5% cRGD-decorated CCPM, to localize in close proximity to cell nuclei (**Fig. 5B**), further corroborating the notion of efficient integrin-mediated CCPM cellular internalization. Additional images acquired via multiphoton microscopy in which 4T1 cells were additionally stained with phalloidin to

visualize actin filaments (**Fig. 5C**, green), clearly displayed red clusters of cRGD-modified CCPM to localize in the cytosolic perinuclear space. These observations were in line with others in literature,e.g. using 5% cRGD nanocarriers in MDA-MB-231 cells [47].

The quantification of rhodamine AF% on fluorescence live cell imaging (**Fig. 5D**) confirmed the preceding data obtained using fluorescence microscopy in fixed cells (**Fig. 1, 2**), with cRGD-CCPM binding being positively affected by increasing amounts of cRGD decoration. Of note, the quantification of lysotracker AF% also follows a similar increasing trend as rhodamine nanoparticles, with more lysotracker signal being quantified upon increased uptake of nanoparticles. Because recent evidences show the ability of cells to increase the number of lysosomes in reponse to degradative or energetic needs, it is reasonable to speculate that increased uptake of nanomaterial may be reflected into an increased number of endosomes and lysosomes [48]. Higher-resolution imaging modalities, such as super-resolution STED (for live or fixed cells) or electron microscopy (for fixed cells only), combined with more specific lysosome-stainings such as LAMP-1, would be suitable tools to further study whether an increase in lysosome numbers indeed occurs upon enhanced uptake of CCPM.

Finally, we also studied the internalization of cRGD-decorated CCPM by flow cytometry. This analysis confirmed that the association of cRGD-CCPM (1, 3.6, and 5 mol%) with 4T1 cells upon incubation for 24 h at 37 ^{o}C was significantly higher than that of cRGD-free control CCPM. The mean fluorescence intensity values (MFI) of 357, 424, 433, and 435 were obtained for the 0, 1, 3.6, and 5 mol% cRGD CCPM, respectively (**Fig. 5E**).

Identifying the optimal cRGD decoration density for follow-up in vivo studies

Cyclic RGD is among the most widely studied targeting ligand and it has demonstrated strong affinities for $\alpha_v\beta_3$ integrin, a key receptor expressed by multiple cell populations including among others, cancer cells of the skin and of the breast, endothelial cells and neutrophils. Surface functionalization of nanoparticles with targeting ligands such as cRGD has shown significant advantages in preclinical cancer nanotherapy studies [49,50]. However, in-depth cellular examination already revealed that RGD-targeting induced nanoparticle association with tumor vasculature while marginally reaching the tumor interstitium [29,51]. In addition, in the bloodstream, targeting moieties present on the nanoparticle surface may cause elevated recognition by the mononuclear phagocyte system (MPS) and thereby compromise nanoparticle PK characteristics and tumor accumulation [13,33,47]. Thus, it is key to identify the right decoration density to balance the increased uptake efficacy and good PK prolifes for in vivo applications.

For identifying the benefit of cRGD decoration, we quantitively compared the binding and internalization of the various CCPM formulations by both the $\alpha_v\beta_3$-integrin^{high} cell types used (4T1,TNFα-activated HUVEC) and at all available experiments. For 4T1 cell line, five experiments involved incubation of these cells with all four CCPM formulations, including incubation assay for 4, 24, 72 h at 37^{o}C and evaluation via fluorescence microscopy (**Fig. 2, 3**), internalization assay for 24 h at 37^{o}C and evaluation via multiphoton microscopy (**Fig. 5D**), and finally quantification of the uptake extent after incubation for 24 h

at 37^{o}C via flow cytometry (**Fig. 5E**). For HUVEC^{+}, three experiments entailed the incubation of the cells with all four CCPM formulations, i.e., incubation assay for 4, 24, and 72 h at 37^{o}C and evaluation via fluorescence microscopy (**Fig. 2, 3**).

By comparing the binding / uptake values for each nanoformulation at these experiments, and by normalizing these values based on the binding / uptake of control CCPM (0 mol% cRGD) for each individual experiment, we displayed the enhanced uptake ratio for each formulation for each different experiment (**Fig. 6**). For 4T1 cells, the uptake increase ratio ranged between 1.2-1.5, 1.2-1.7, and 1.2-2.3 for the 1, 3.6, and 5% cRGD CCPM (**Fig. 6A,B**). Considering the additional 20-50% uptake due to the 1% cRGD decoration, from a theoretical and proportional point of view, the 3.6 and 5% cRGD CCPM should result into an additional uptake comprised between 72-180% and 100-250%, respectively. Analysis of our data set reveals instead that a decoration density of 3.6 and 5% cRGD resulted in an additional uptake between 20-70% and 20-130% by 4T1 cells as compared to control CCPM. For HUVEC^{+} cells, the uptake increase ratio ranged between 1.3-2.2, 2.1-3.2, and 2.6-4.0 for the 1, 3.6, and 5% cRGD CCPM (**Fig. 6C,D**). Similarly to the abovementioned calculations, the additional uptake due to the 1% cRGD decoration was of 30-120%, and it should theoretically be within the range of 108-432%, and 150-600%, for the 3.6 and 5% cRGD CCPM, respectively, if the increase in the cRGD would be accompanied by a proportional increase in uptake by target cells. However, the additional increase ranged at the lower end of the theoretical values, i.e., 110-220% and 160-300% for the 3.6 and 5% cRGD CCPM, respectively.Such observation indicates that increasing the decoration density does not necessarily contribute to a proportional increase in binding and/or uptake. Besides by particle size and charge, several studies have evidenced that surface decoration with targeting ligands modulates BD profiles [33,47,52]. For example, high cRGD decoration density can shift the accumulation of nanoparticles to the RES system and reduce the nanoparticle availability for targeting purposes, thus, requiring an additional PEG-shielding for ameliorating this effect [47]. In addition, high amounts of ligand decoration may promote unwanted protein corona formation, with opsonization in the blood and uptake by phagocytes in liver and spleen [33]. Finally, high concentrations of cRGD might negatively modulate the downstream signaling events, such as a loss in cadherin-dependent intercellular contacts [53].Of note, also the clinical trialing of cRGD in the form of a cRGD-decorated silica nanoparticles was done via a low functionalization as only 6-7 cRGD molecules were added per particle. This choice was specifically done for maintaining a small hydrodynamic size, that would not significantly shift the BD profile of the evaluated diagnostic nanoparticle [54]. In addition, it is important to state that CCPM is a formulation with negligible formation of protein corona [55], therefore low decoration densities might be suitable for maintaining this desirable feature for prolonged circulation and efficient tumour targeting. In addition, we [13,18,31] and others [23,44,51,56] have observed that low decoration densities (i.e., 1 mol% or lower) are sufficient for significantly altering the in vivo behavior between ligand-decorated and non-decorated analogues.

Taken together, by comparing the in vitro uptake patterns in the $\alpha_v\beta_3$-integrin^{high} cell lines, and considering previous observations from in vivo and clinical set-ups where cRGD decorations were used, we suggest that low decoration densities (in the range of 1 mol%) are sufficient to beneficially alter the

targeting behavior of the formulations, but not too high for causing deleterious effects on their in vivo behavior (i.e., improper PK and extensive deposition in clearance organs).

Summarizing Discussion

The present study aimed at expanding our understanding of the effect of ligand decoration densities on the active targeting properties of clinical-stage platform based on core-crosslinked polymeric micelles (CCPM). In this regard, we evaluated the uptake of rhodamine-labelled CCPM decorated with increasing cRGD densities (1, 3.6 and 5 mol%) against $\alpha_v\beta_3$-integrin^{high} (i.e., 4T1 breast cancer and TNFα- activated HUVEC), $\alpha_v\beta_3$-integrin^{low} cells (i.e., A431 epidermoid carcinoma cell line), and $\alpha_v\beta_3$-integrin^{intermediate} cells (non-activated HUVEC).

Our results show that: (**i**) the uptake of cRGD CCPM is time- and temperature-dependent, with the optimal uptake condition registered at 24 h post incubation at 37°C; that (**ii**) the uptake efficacy of cRGD CCPM is higher in $\alpha_v\beta_3$-integrin^{high} cells, both under static and dynamic cultivation conditions, thereby confirming the functionality and additional benefit of the ligand; that (**iii**) cRGD CCPM are more efficiently internalized by target cells as compared to control CCPM and localize in proximity to cell nuclei; also, internalized particles co-localize with lysosomes, thus highlighting the additional efficacy of exploiting $\alpha_v\beta_3$ integrin-based internalization strategies; and that (**iv**) the increase in cRGD decoration density does not result in a proportional increase in the uptake of functionalized CCPM, suggesting that relatively low decoration densities in the range of 1 mol% cRGD may already be sufficient for evoking a change in CCPM targeting and uptake in vivo.

Concerning the selection of a relatively low cRGD mol% decoration for eventual in vivo experimentation, it should be kept in mind that the extensive presence of targeting ligands may affect the PK and BD profile of nanonomedicines. Besides by particle size and charge, several studies have evidenced that surface decoration with targeting ligands modulates BD profiles [33, 47, 52]. For example, high cRGD decoration density can shift the accumulation of nanoparticles to the RES system and reduce the nanoparticle availability for targeting purposes, thus, requiring an additional PEG-shielding for ameliorating this effect [47]. In addition, high amounts of ligand decoration may promote unwanted protein corona formation, with opsonization in the blood and uptake by phagocytes in liver and spleen [33]. Finally, high concentrations of cRGD might negatively modulate the downstream signaling events, such as a loss in cadherin-dependent intercellular contacts [53].

Conclusion

Using static and dynamic cultivation studies, we profiled the cellular uptake of actively targeted core-crosslinked polymeric micelles in vitro. Our results showed benefit of active targeting with respect to the internalization of CCPM by target cells. Comparing the three cRGD-decorated nanoformulations tested, the highest decoration density (5 mol % cRGD) resulted in the highest uptake and internalization rate of CCPM by targeted cells, under all experimental conditions tested. However, in depth analysis evidenced

that increasing the decoration density does not necessarily contribute to a proportional increase in binding and/or uptake. Taken into account that it is key to identify the right decoration density, we suggest that low decoration densities are capable of improving the cell targeting of formulations, but not too high to cause detrimental effects on their in vivo behavior.

Declarations

Ethics approval and consent to participate

Not applicable

Consent for publication

All authors approve the publication

Availability of data and materials

Raw data are available by the authors upon request

Competing interests

QH, MT, CJFR are employees of Cristal Therapeutics. The other authors declare no competing interests.

Funding

The authors gratefully acknowledge financial support by the European Fund for Regional Development (FDL, AM, TL – TAKTIRA: Project number: EFRE-0801767)), the European Research Council (RD, TL – ERC Consolidator Grant 864121: Meta-Targeting), the German Research Foundation (TL – DFG: GRK2375 (Project number: 331065168); AMS – DFG RWTH JPI Excellence Initiative; LK – CRC1066 grant for projects B03, B04; LK, TL, AMS – CRC1066 grant for project B17), the German Federal Ministry of Research and Education (TL; BMBF: Gezielter Wirkstofftransport, PP-TNBC, Project number 16GW0319K), and the German Cancer Aid (AMS – SDK Postgraduate Program MSSOABCD).

Authors' contribution

FDL, CJFR, LYR, and TL conceptualized the study. FDL, LYR, and TL designed the experiments. LYR, LC, FK, AMS, and TL supervised the study. QH, MT, and CJFR produced the nanoformulations. FDL executed all the in vitro and fluorescence microscopy experiments. MBau, MV, MvZ, and FDL executed the two-photon microscopy acquisition. FDL and MBar performed the flow cytometry experiment. FDL analyzed and quantified all data. FDL and AMS produced the figures. FDL, RD, AM, LK, AMS, and TL wrote the manuscript. All authors read, revised, and approved the manuscript.

Acknowledgements

This work was actively supported by the Core Facility “Two-Photon Imaging”, a Core Facility of the Interdisciplinary Center for Clinical Research (IZKF) Aachen within the Faculty of Medicine at RWTH Aachen University.

References

1. Talelli M, Barz M, Rijcken CJ, Kiessling F, Wim E. Core-Crosslinked Polymeric Micelles: Principles, Preparation, Biomedical Applications and Clinical Translation. Nano Today. 2015;10:93–117.
2. Shi Y, van der Meel R, Theek B, Oude Blenke E, Pieters EHE, Fens MHAM, et al. Complete Regression of Xenograft Tumors upon Targeted Delivery of Paclitaxel *via* Π–Π Stacking Stabilized Polymeric Micelles. ACS Nano American Chemical Society. 2015;9:3740–52.
3. Hu Q, Rijcken CJF, van Gaal E, Brundel P, Kostkova H, Etrych T, et al. Tailoring the physicochemical properties of core-crosslinked polymeric micelles for pharmaceutical applications. J Control Release [Internet]. Elsevier B.V.; 2016;244:314–25. Available from: http://dx.doi.org/10.1016/j.jconrel.2016.07.012.
4. Rijcken CJ, Snel CJ, Schiffelers RM, Nostrum CF, Van, Hennink WE. Hydrolysable core-crosslinked thermosensitive polymeric micelles: Synthesis, characterisation and in vivo studies. 2007;28:5581–93.
5. Hu Q, Rijcken CJ, Bansal R, Hennink WE, Storm G, Prakash J. Complete regression of breast tumour with a single dose of docetaxel-entrapped core-cross-linked polymeric micelles. Biomaterials [Internet]. Elsevier Ltd; 2015;53:370–8. Available from: http://dx.doi.org/10.1016/j.biomaterials.2015.02.085.
6. Biancacci I, Sun Q, Möckel D, Gremse F, Rosenhain S, Kiessling F, et al. Optical imaging of the whole-body to cellular biodistribution of clinical-stage PEG-b-pHPMA-based core-crosslinked polymeric micelles. J Control Release [Internet]. Elsevier B.V; 2020;328:805–16. Available from: https://doi.org/10.1016/j.jconrel.2020.09.046.
7. Atrafi F, van Eerden RAG, van Hylckama Vlieg MAM, Hoop EO, de Bruijn P, Lolkema MP, et al. Intratumoral Comparison of Nanoparticle Entrapped Docetaxel (CPC634) with Conventional Docetaxel in Patients with Solid Tumors. Clin Cancer Res. 2020;26:3537–45.
8. Atrafi F, Dumez H, Mathijssen RHJ, Menke van der Houven van Oordt CW, Rijcken CJF, Hanssen R, et al. A phase I dose-escalation and pharmacokinetic study of a micellar nanoparticle with entrapped docetaxel (CPC634) in patients with advanced solid tumours. J Control Release [Internet]. Elsevier; 2020;325:191–7. Available from: https://doi.org/10.1016/j.jconrel.2020.06.020.
9. Atrafi F, van Eerden RAG, Koolen SLW, de Bruijn P, Rijcken CJF, Hanssen R, et al. Docetaxel skin exposure and micronucleation contributes to skin toxicity caused by cpc634. Cancers (Basel). 2021;13.
10. Matsumura Y, Maeda H. A new concept for macromolecular therapeutics in cancer chemotherapy: mechanism of tumoritropic accumulation of proteins and the antitumor agent smancs. Cancer Res American Association for Cancer Research. 1986;46:6387–92.

11. Naumenko VA, Vlasova KY, Garanina AS, Melnikov PA, Potashnikova DM, Vishnevskiy DA, et al. Extravasating Neutrophils Open Vascular Barrier and Improve Liposomes Delivery to Tumors. ACS Nano. 2019;13:12599–612.
12. Matsumoto Y, Nichols JW, Toh K, Nomoto T, Cabral H, Miura Y, et al. Vascular bursts enhance permeability of tumour blood vessels and improve nanoparticle delivery. Nat Nanotechnol Nature Publishing Group. 2016;11:533–8.
13. Sofias AM, Toner YC, Meerwaldt AE, Van Leent MMT, Soultanidis G, Elschot M, et al. Tumor Targeting by αvβ3-Integrin-Specific Lipid Nanoparticles Occurs via Phagocyte Hitchhiking. ACS Nano. 2020;14:7832–46.
14. Sindhwani S, Syed AM, Ngai J, Kingston BR, Maiorino L, Rothschild J, et al. The entry of nanoparticles into solid tumours. Nat Mater [Internet]. Springer US; 2020;19:566–75. Available from: http://dx.doi.org/10.1038/s41563-019-0566-2.
15. Miller MA, Zheng YR, Gadde S, Pfirschke C, Zope H, Engblom C, et al. Tumour-associated macrophages act as a slow-release reservoir of nano-therapeutic Pt(IV) pro-drug. Nat Commun. Nature Publishing Group; 2015;6.
16. Rosenblum D, Joshi N, Tao W, Karp JM, Peer D. Progress and challenges towards targeted delivery of cancer therapeutics. Nat Commun [Internet]. Springer US; 2018;9. Available from: http://dx.doi.org/10.1038/s41467-018-03705-y.
17. Zhao Z, Ukidve A, Kim J, Mitragotri S. Targeting Strategies for Tissue-Specific Drug Delivery. Cell [Internet]. Elsevier Inc.; 2020;181:151–67. Available from: https://doi.org/10.1016/j.cell.2020.02.001.
18. Sofias AM, Andreassen T, Hak S. Nanoparticle Ligand-Decoration Procedures Affect in Vivo Interactions with Immune Cells. Mol Pharm. 2018;15:5754–61.
19. Hak S, Helgesen E, Hektoen HH, Huuse EM, Jarzyna PA, Mulder WJM, et al. The effect of nanoparticle polyethylene glycol surface density on ligand-directed tumor targeting studied in vivo by dual modality imaging. ACS Nano. 2012;6:5648–58.
20. Sieber S, Grossen P, Uhl P, Detampel P, Mier W, Witzigmann D, et al. Zebrafish as a predictive screening model to assess macrophage clearance of liposomes in vivo. Nanomedicine Nanotechnology, Biol Med [Internet]. Elsevier Inc; 2019;17:82–93. Available from: https://doi.org/10.1016/j.nano.2018.11.017.
21. Elias DR, Poloukhtine A, Popik V, Tsourkas A. Effect of ligand density, receptor density, and nanoparticle size on cell targeting. Nanomedicine Nanotechnology, Biol Med [Internet]. Elsevier Inc.; 2013;9:194–201. Available from: http://dx.doi.org/10.1016/j.nano.2012.05.015.
22. Danhier F, Vroman B, Lecouturier N, Crokart N, Pourcelle V, Freichels H, et al. Targeting of tumor endothelium by RGD-grafted PLGA-nanoparticles loaded with Paclitaxel. J Control Release Elsevier. 2009;140:166–73.
23. Phillips E, Penate-Medina O, Zanzonico PB, Carvajal RD, Mohan P, Ye Y, et al. Clinical translation of an ultrasmall inorganic optical-PET imaging nanoparticle probe. Sci Transl Med. 2014;6:1–10.

24. Benezra M, Phillips E, Overholtzer M, Zanzonico PB, Tuominen E, Wiesner U, et al. Ultrasmall integrin-targeted silica nanoparticles modulate signaling events and cellular processes in a concentration-dependent manner. Small. 2015;11:1721–32.
25. Liu CH, Chern GJ, Hsu FF, Huang KW, Sung YC, Huang HC, et al. A multifunctional nanocarrier for efficient TRAIL-based gene therapy against hepatocellular carcinoma with desmoplasia in mice. Hepatology. John Wiley and Sons Inc.; 2018;67:899–913.
26. Amin M, Mansourian M, Koning GA, Badiee A, Jaafari MR, Ten Hagen TLM. Development of a novel cyclic RGD peptide for multiple targeting approaches of liposomes to tumor region. J Control Release [Internet]. Elsevier B.V.; 2015;220:308–15. Available from: http://dx.doi.org/10.1016/j.jconrel.2015.10.039.
27. De La Rosa R, Spadea JM, Donno A, Lallana R, Lu E, Puri Y. S, et al. Microfluidic-assisted preparation of RGD-decorated nanoparticles: exploring integrin-facilitated uptake in cancer cell lines. Sci Rep. 2020;10:1–15.
28. Wang F, Li Y, Shen Y, Wang A, Wang S, Xie T. The functions and applications of RGD in tumor therapy and tissue engineering. Int J Mol Sci. 2013;14:13447–62.
29. Cai W, Shin DW, Chen K, Gheysens O, Cao Q, Wang SX, et al. Detection of tumor angiogenesis in vivo by alphaVbeta3-targeted magnetic resonance imaging. Nat Med. 2007;6:1555–62.
30. Schnittert J, Bansal R, Storm G, Prakash J. Integrins in wound healing, fibrosis and tumor stroma: High potential targets for therapeutics and drug delivery. Adv Drug Deliv Rev Elsevier B V. 2018;129:37–53.
31. Sofias AM, Bjørkøy G, Ochando J, Sønstevold L, Hegvik M, de L Davies, Haraldseth C, Lammers O, Mulder T, Hak WJM. S. Cyclic Arginine–Glycine–Aspartate-Decorated Lipid Nanoparticle Targeting toward Inflammatory Lesions Involves Hitchhiking with Phagocytes. Adv Sci [Internet]. 2021;8:2100370. Available from: doi: 10.1002/advs.202100370.
32. Fay F, Hansen L, Hectors SJCG, Sanchez-gaytan BL, Zhao Y, Tang J, et al. HHS Public Access. 2017;28:1413–21.
33. Kunjachan S, Pola R, Gremse F, Theek B, Ehling J, Moeckel D, et al. Passive versus active tumor targeting using RGD- and NGR-modified polymeric nanomedicines. Nano Lett. 2014;14:972–81.
34. Hu Q. Core-cross-linked polymeric micelles: a versatile nanomedicine platform with broad applicability. Enschede: University of Twente; 2015.
35. Swerlick RA, Lee K, Li L-J, Sepp NT, Caughman Wright S, Lawley TJ. Regulation of vascular cell adhesion molecule 1 on human dermal microvascular endothelial cells. J Immunol. 1991;149:698–705.
36. Zhang C, Jugold M, Woenne EC, Lammers T, Morgenstern B, Mueller MM, et al. Specific targeting of tumor angiogenesis by RGD-conjugated ultrasmall superparamagnetic iron oxide particles using a clinical 1.5-T magnetic resonance scanner. Cancer Res. 2007;67:1555–62.
37. Haubner R, Weber WA, Beer AJ, Vabuliene E, Reim D, Sarbia M, et al. Noninvasive visualization of the activated αvβ3 integrin in cancer patients by positron emission tomography and [18F]Galacto-RGD.

PLoS Med. 2005;2:0244–52.

38. Swerlick RA, Lee K, Li L-J, Sepp NT, Caughman Wright S, Lawley TJ. REGULATION OF VASCULAR CELL ADHESION MOLECULE 1 ON HUMAN DERMAL MICROVASCULAR ENDOTHELIAL CELLS. J Immunol. 1991;149:698–705.
39. Schmid SL, Carter LL, Smythe E. ATP is Required for Receptor-Mediated Endocytosis Both in Vivo and in Vitro. Endocytosis. 1992;111:105–11.
40. Gao B, Saba TM, Tsan M, Saba TM, Tsan M. Role of_v_3-integrin in TNF-_-induced endothelial cellmigration. Am J Physiol Cell Physiol. 2002;283:1196–205.
41. Sipkins DA, Cheresh DA, Kazemi MR, Nevin LM, Berdnarski MD, Li KCP. Detection of tumor angiogenesis in vivo by alphaVbeta3-targeted magnetic resonance imaging. Nat Med. 1998;4:623–6.
42. Cai W, Shin DW, Chen K, Gheysens O, Cao Q, Wang SX, et al. Peptide-labeled near-infrared quantum dots for imaging tumor vasculature in living subjects. Nano Lett. 2006;6:669–76.
43. Zhang C, Jugold M, Woenne EC, Lammers T, Morgenstern B, Mueller MM, et al. Specific targeting of tumor angiogenesis by RGD-conjugated ultrasmall superparamagnetic iron oxide particles using a clinical 1.5-T magnetic resonance scanner. Cancer Res. 2007;67:1555–62.
44. Montet X, Montet-Abou K, Reynolds F, Weissleder R, Josephson L. Nanoparticle imaging of integrins on tumor cells. Neoplasia. 2006;8:214–22.
45. Mellman I, Yarden Y. Endocytosis and cancer. Cold Spring Harb Perspect Biol. 2013;5.
46. Paul NR, Jacquemet G, Caswell PT. Endocytic Trafficking of Integrins in Cell Migration. Curr Biol Cell Press. 2015;25:R1092–105.
47. Fay F, Hansen L, Hectors SJCG, Sanchez-Gaytan BL, Zhao Y, Tang J, et al. Investigating the Cellular Specificity in Tumors of a Surface-Converting Nanoparticle by Multimodal Imaging. Bioconjug Chem. 2017;28:1413–21.
48. Foret L, Dawson JE, Villaseñor R, Collinet C, Deutsch A, Brusch L, et al. A general theoretical framework to infer endosomal network dynamics from quantitative image analysis. Curr Biol. 2012;22:1381–90.
49. Arosio D, Casagrande C. Advancement in integrin facilitated drug delivery. Adv Drug Deliv Rev Elsevier B V. 2016;97:111–43.
50. Sheikh A, Alhakamy NA, Md S, Kesharwani P. Recent Progress of RGD Modified Liposomes as Multistage Rocket Against Cancer. Front Pharmacol. 2022;12:1–19.
51. Smith BR, Cheng Z, De A, Rosenberg J, Gambhir SS. Dynamic visualization of RGD-quantum dot binding to tumor neovasculature and extravasation in multiple living mouse models using intravital microscopy. Small. 2010;6:2222–9.
52. Ernsting MJ, Murakami M, Roy A, Li S-D. Factors Controlling the Pharmacokinetics, Biodistribution and Intratumoral Penetration of Nanoparticles. J Control Release [Internet]. 2013;172:782–794. Available from: https://www.ncbi.nlm.nih.gov/pmc/articles/PMC3624763/pdf/nihms412728.pdf.

53. Kiessling F, Uppert J, Zhang C, Jayapaul J, Zwick S, Woenne EC, et al. RGD-labeled USPIO Inhibits Adhesion and Endocytotic Activity of _v3-Integrin–expressing Glioma Cells and Only Accumulates in the Vascular Tumor Compartment. Radiology. 2009;253:462–9.
54. Benezra M, Penate-Medina O, Zanzonico PB, Schaer D, Ow H, Burns A, et al. Multimodal silica nanoparticles are effective cancer-targeted probes in a model of human melanoma. J Clin Invest. 2011;121:2768–80.
55. Alberg I, Kramer S, Schinnerer M, Hu Q, Seidl C, Leps C, et al. Polymeric Nanoparticles with Neglectable Protein Corona. Small. 2020;16.
56. Tsvetkova Y, Beztsinna N, Baues M, Klein D, Rix A, Golombek SK, et al. Balancing Passive and Active Targeting to Different Tumor Compartments Using Riboflavin-Functionalized Polymeric Nanocarriers. Nano Lett. 2017;17:4665–74.

Figures

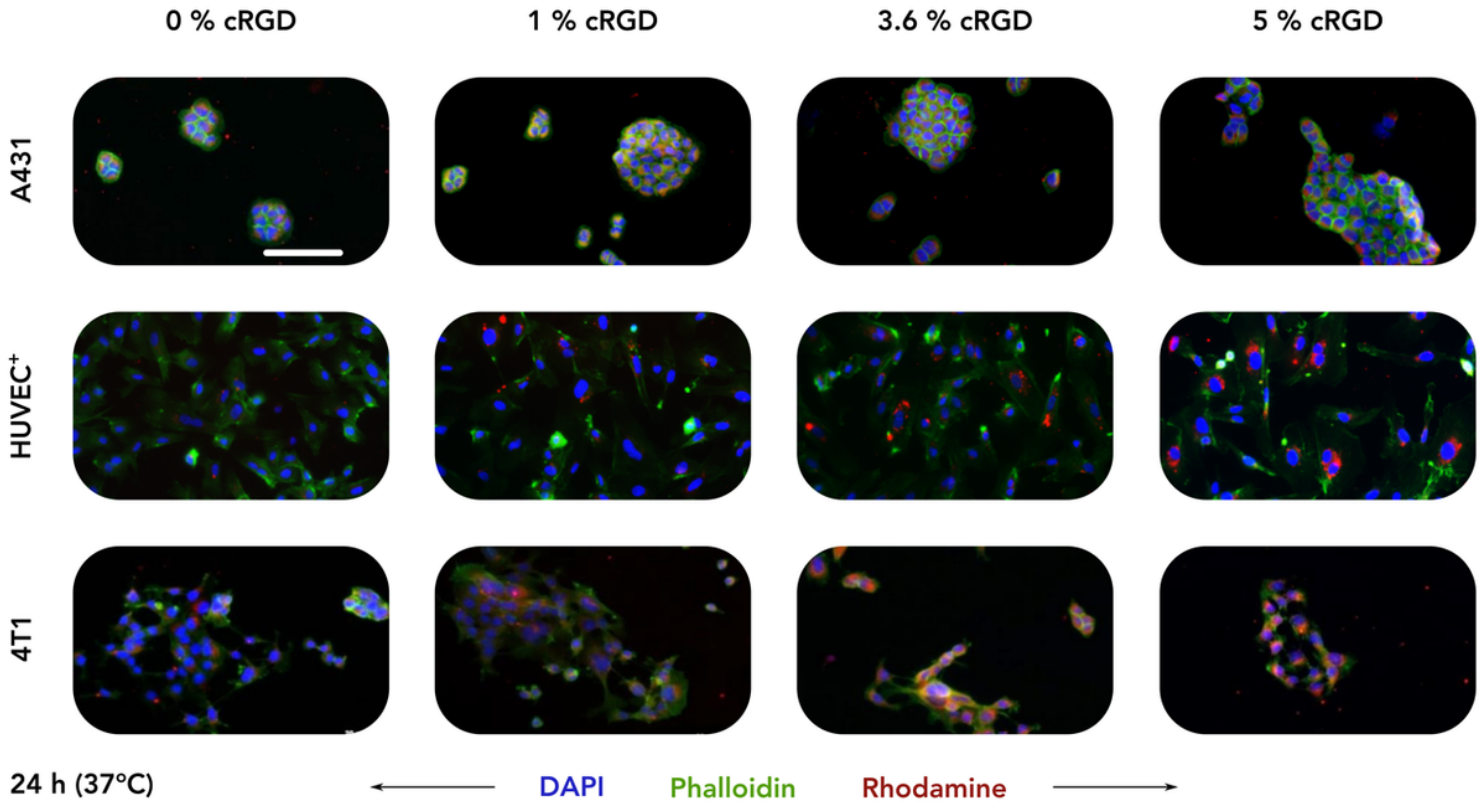

Figure 1

Uptake of control and cRGD-decorated CCPM after 24 h of incubation at 37°C. Representative fluorescence microscopy images depict the uptake of rhodamine-labelled control and cRGD-targeted (1, 3.6 and 5 mol%) CCPM by A431 (human squamous carcinoma), TNFα-activated HUVEC (HUVEC^{+}), and 4T1 (murine triple-negative breast cancer) cells 24 h post incubation, at 37°C. All four nanoparticle formulation are taken up to a similar extent by A431 cells ($\alpha_v\beta_3$-integrin^{negative} cell line), while increasing

the cRGD-decoration density results in an enhanced uptake by HUVEC^{+} and 4T1 cells ($\alpha_v\beta_3$-integrin^{positive} cell lines). Color coding: DAPI (nuclei; blue), phalloidin (actin filaments; green), and rhodamine (micelles, red). Scale bar = 100 µm.

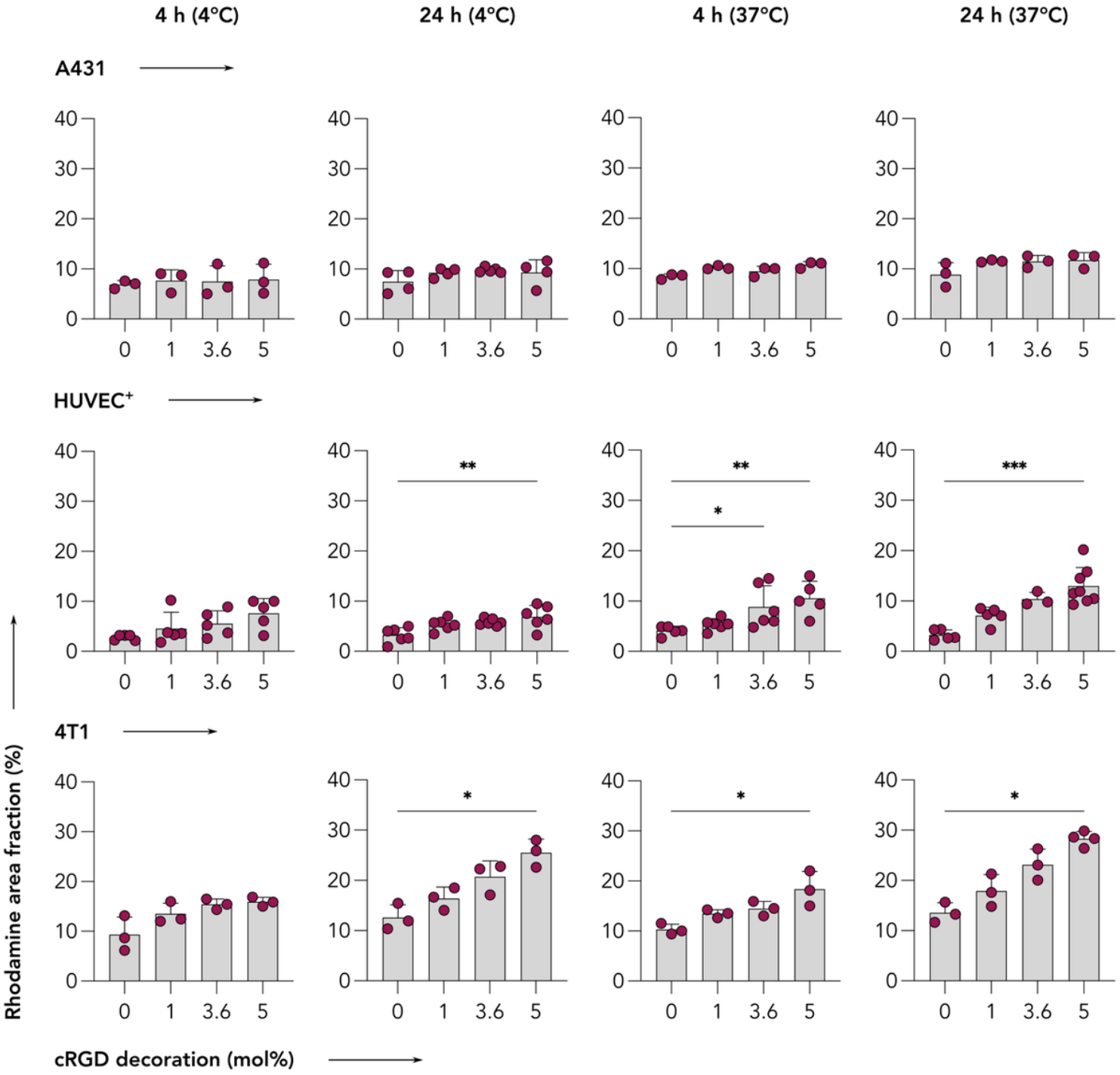

Figure 2

cRGD-decorated CCPM display time-, temperature- and ligand density-dependent uptake in $\alpha_v\beta_3$ integrin-expressing cells. Quantification of the uptake (i.e., rhodamine area fraction %) of control and cRGD-

decorated micelles from fluorescence microscopy images (raw images presented in Fig. 1, S2, S3 and S4) reveals that all four nanoparticle formulations are taken up to similar extent by A431 cells ($\alpha_v\beta_3$-integrin^{negative} cell line). Conversely, increasing the incubation time, incubation temperature and cRGD density results in enhanced uptake by TNFα-activated HUVEC (HUVEC^{+}) and 4T1 ($\alpha_v\beta_3$-integrin^{positive}) cells**.** Data are presented as mean ± standard deviation of n=3-7 biological replicates. Level of significance was assessed by a Kruskal-Wallis one-way ANOVA test, followed by Dunn´s multiple comparison correction test. P-values: *< 0.05; **< 0.01, and ***< 0.001.

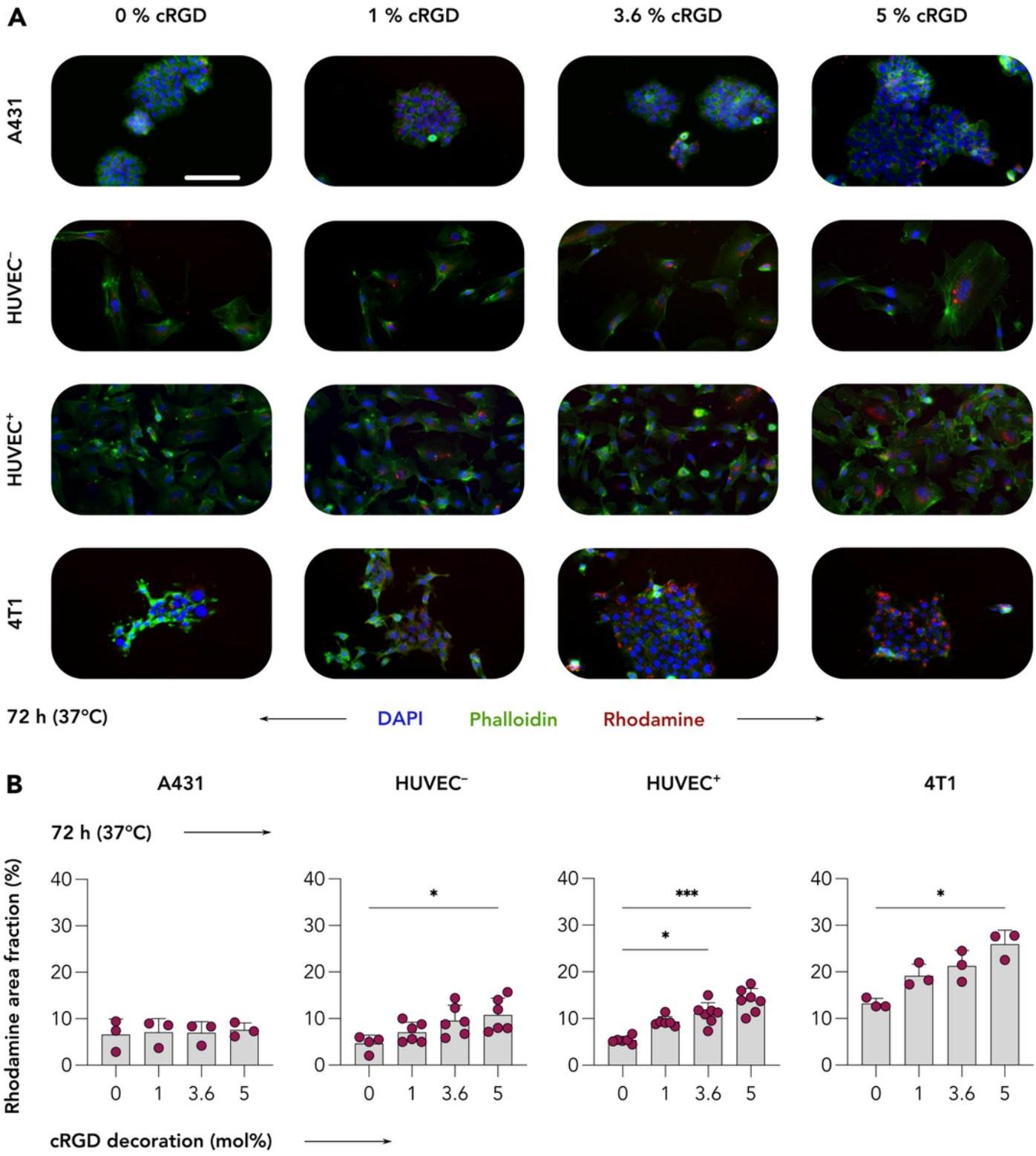

Figure 3

Uptake of control and cRGD-decorated CCPM by A431, HUVEC and 4T1 cells after 72 h incubation. A. Representative fluorescence microscopy images showing the uptake of control and cRGD-decorated micelles by A431, quiescent HUVEC (HUVEC$^-$), TNFα-activated HUVEC (HUVEC$^+$), and 4T1 cells at 72 h post incubation at 37^{o}C. Color coding: DAPI (nuclei, blue), phalloidin (actin filaments, green), and rhodamine (CCPM, red). Scale bar = 100 μm. **B.** All four CCPM formulations are similarly taken up by

A431 cells ($\alpha_v\beta_3$-integrin^{negative}), while increasing the cRGD-decoration density promotes uptake by HUVEC and 4T1 cells (i.e. all three $\alpha_v\beta_3$-integrin^{positive} cell lines). Importantly,TNFα -activated HUVEC display higher CCPM internalization in comparison to the non-activated cell line. Data are presented as mean ± SD. N=3-7 biological replicates. Levels of significance were assessed by using a Kruskal-Wallis one-way ANOVA followed by Dunn´s multiple comparison correction test. *P < 0.05; **P < 0.01, and ***P < 0.001.

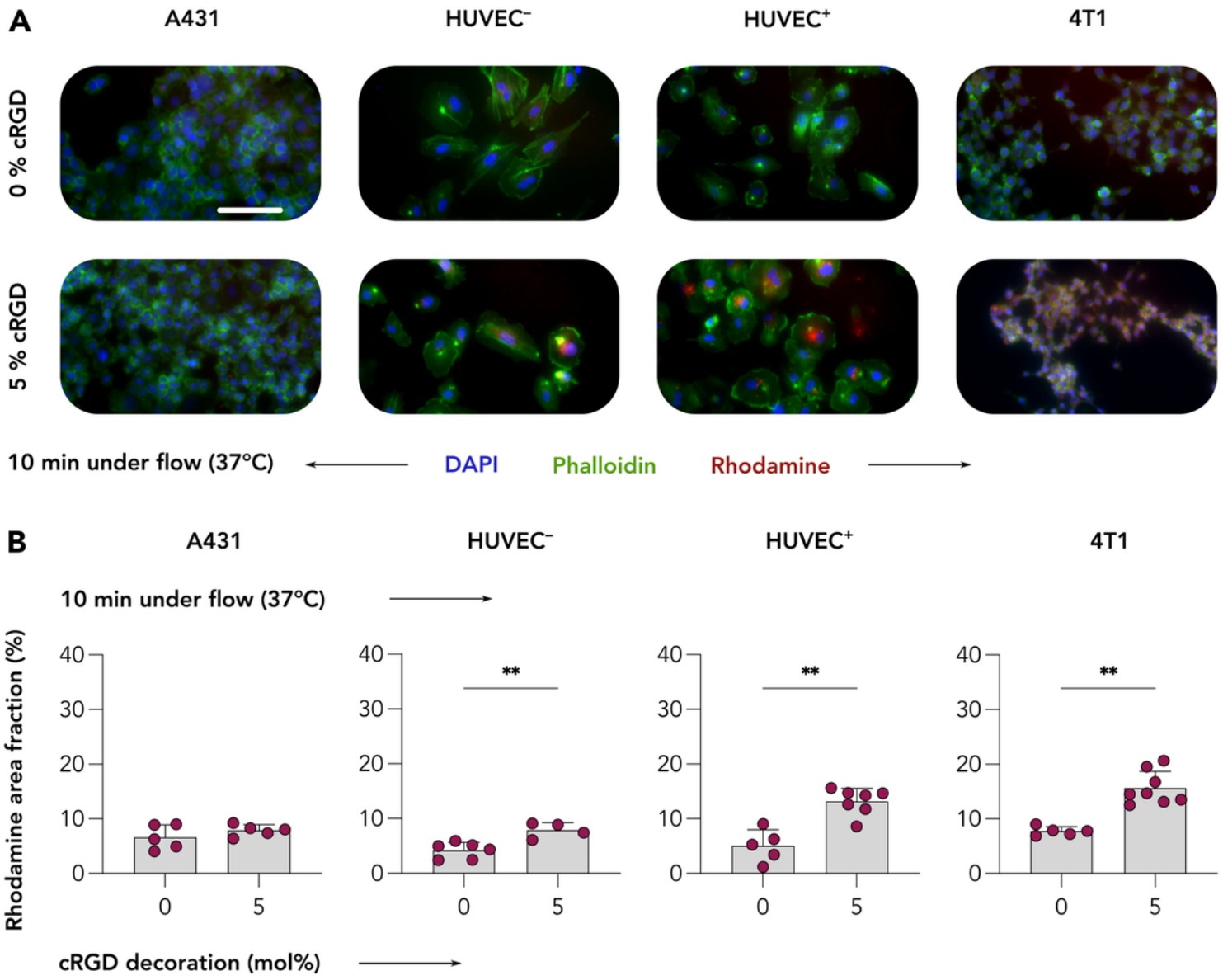

Figure 4

Uptake of control and cRGD-decorated CCPM upon 10 min of incubation under flow conditions. A. Representative fluorescent microscopy images displaying A431, quiescent (HUVEC$^-$), and TNFα-activated (HUVEC$^+$) HUVEC, as well as 4T1 cells following incubation with control and 5% cRGD-targeted CCPM under physiological fluid flow for 10 min at 37 ^oC. Color coding: DAPI (nuclei, blue), phalloidin (actin filaments, green), and rhodamine (CCPM, red). Scale bar = 100 µm. **B.** Quantification of CCPM uptake (i.e.,

rhodamine area fraction %) shows a 3-fold increase in the uptake of cRGD-targeted CCPM by $\alpha_v\beta_3$ integrin-positive cells as compared to control CCPM, exemplifying that cRGD efficiently and rapidly mediates cellular uptake? under shear stress conditions. Data are presented as mean ± SD. N = 5-8 biological replicates. Levels of significance were assessed by a Mann-Whitney´s non-parametric two-tailed. P-values: **< 0.01.

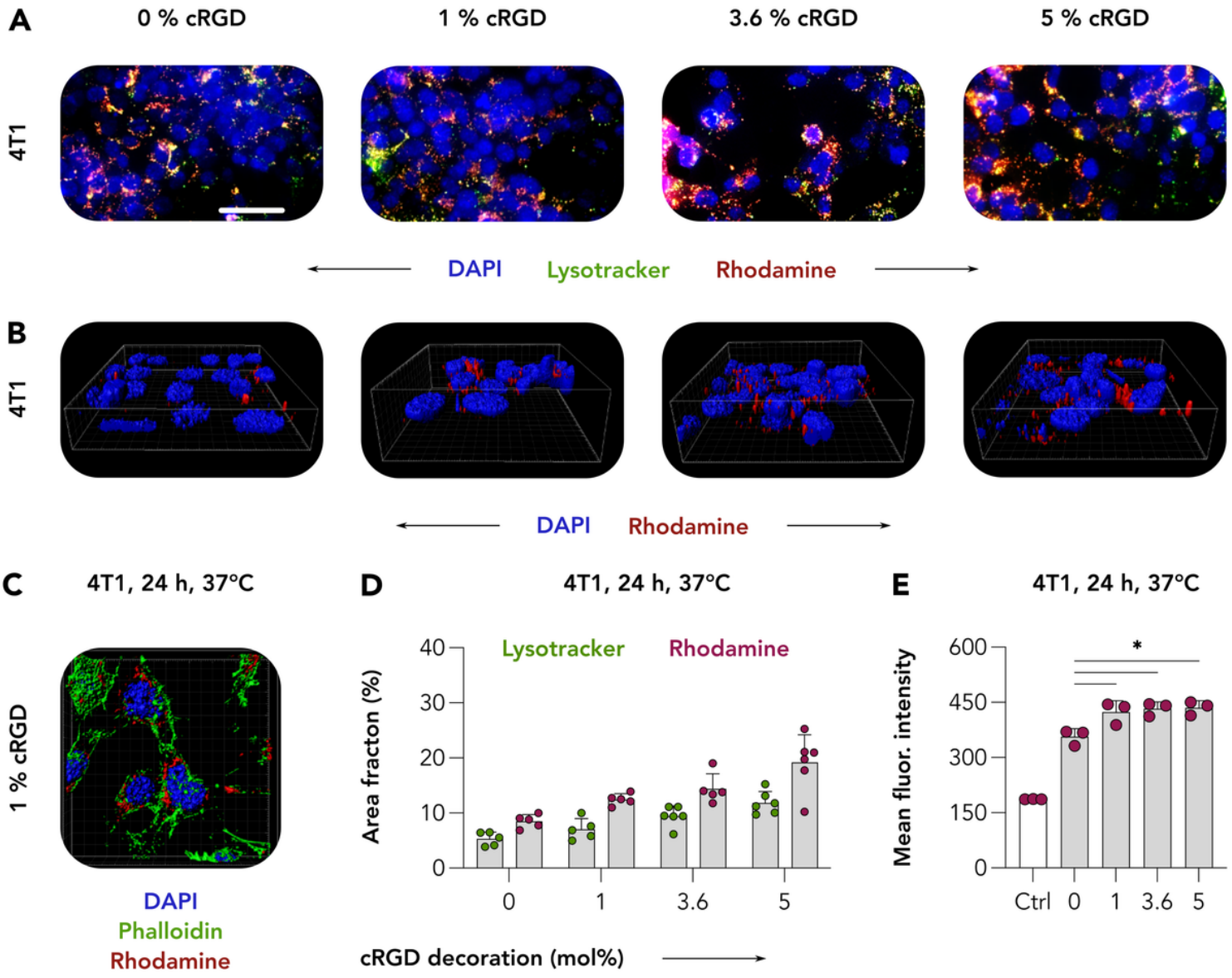

Figure 5

Internalization of cRGD-decorated CCPM. A. 4T1 breast cancer cells were incubated with control and cRGD-CCPM for 24 h at 37 °C. Lysotracker® was subquentially added to visualize the endosomal-lysosomal compartment. On live-cell imaging, the co-localization (yellow in merged images) of CCPM (red) with endosomes/lysosomes (green) was suggestive for CCPM internalization. Color coding: DAPI (nuclei, blue), lysotracker® (endo/lysosomes, green), and rhodamine (micelles, red). Scale bar = 100 µm.

B,C. Acquisition of 3D images via two-photon microscopy revealed cRGD-CCPM to be in the perinuclear region, further confirming the cRGD-CCPM internalization by 4T1 cells. Color coding: DAPI (nuclei, blue), phalloidin (actin filaments, green), and rhodamine (micelles, red). **D.** Image analysis shows rhodamine and lysotracker® area fraction % to increase upon the increase of cRGD-decoration density. **E.** Quantification of flow cytometry analysis of micelle binding/uptake by 4T1 cells displays a statistically significant increase in uptake of cRGD-conjugated CCPM in comparison to cRGD-free CCPM. Data are presented as mean ± SD of n=3 biological replicates; levels of significance were assessed by using a one-way ANOVA followed by Tukey´s correction. P-values: * < 0.05.

A CCPM uptake by 4T1 cells at different incubation conditions

Fig.	Condition	0 %	1 %	3.6 %	5 %	0 %	1 %	3.6 %	5 %
		Raw values				Normalized values			
2	4 h (37°C)	10.3	13.5	14.5	18.4	1.0	1.3	1.4	1.8
2	24 h (37°C)	13.5	17.9	21.3	28.3	1.0	1.3	1.7	2.1
3	72 h (37°C)	13.2	19.2	23.1	26.0	1.0	1.5	1.6	2.0
5D	24 h (37°C)	8.5	12.5	14.4	19.2	1.0	1.5	1.7	2.3
5E	24 h (37°C)	356.7	423.5	432.7	435.1	1.0	1.2	1.2	1.2

B Normalized uptake

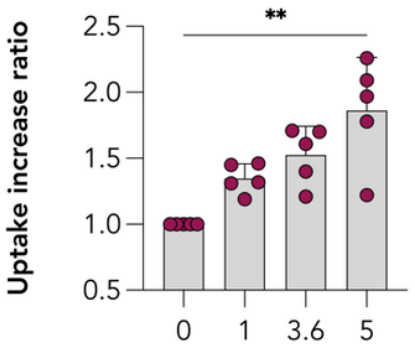

C CCPM uptake by HUVEC⁺ at different incubation conditions

Fig.	Condition	0 %	1 %	3.6 %	5 %	0 %	1 %	3.6 %	5 %
		Raw values				Normalized values			
2	4 h (37°C)	4.1	5.4	8.9	10.6	1.0	1.3	2.2	2.6
2	24 h (37°C)	3.2	7.1	10.4	13.0	1.0	2.2	3.2	4.0
3	72h (37°C)	5.4	9.3	11.1	13.9	1.0	1.7	2.1	2.6

D Normalized uptake

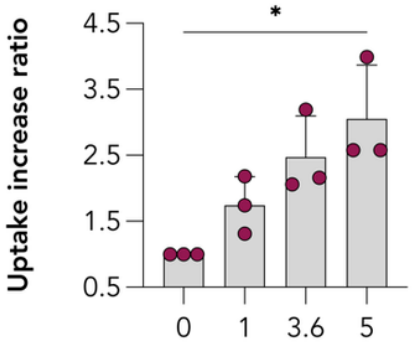

Figure 6

Quantitative comparison of the uptake of control and cRGD-decorated CCPM by $\alpha_v\beta_3$-integrin^{high} cell lines. A,B. Quantification of the uptake of control and cRGD-decorated CCPM by 4T1 cells. **C,D.** Quantification of the uptake of control and cRGD-decorated CCPM by HUVEC⁺. Despite the elevated uptake of the cRGD-decorated CCPM in comparison to control CCPM by both cell lines, the uptake is not proportional to the decoration density. In other words, both 3.6 and 5 mol% decoration does not quantitatively improve the CCPM uptake in comparison to the 1 mol% cRGD decoration. This observation

denotes that higher and higher decoration densities do not result in “inifinite” increases with respect to the formulation binding or uptake.

Supplementary Files

This is a list of supplementary files associated with this preprint. Click to download.

- Graphicalabstract.png
- DeLorenzietal2022Supplementary.docx